

TITLE OF DISSERTATION GOES HERE

Laurel Farris

20 August 2017

Committee:

Dr. R. T. James McAteer
Dr. Jason Jackiewicz
Dr. Nancy Chanover
Dr. Laura Boucheron

Abstract

Abstract text will go here.

CONTENTS

| | |
|--|----|
| 1. Introduction | 1 |
| 2. The solar chromosphere | 5 |
| 2.1. Magnetic field, structure, and the <i>plasma-β</i> | 6 |
| 2.2. Observing the chromosphere | 7 |
| 2.2.1. Characteristic spectral lines/emission | 7 |
| 2.2.2. Challenges | 7 |
| 3. 3-minute oscillations | 8 |
| 3.1. History of 3mOs | 8 |
| 3.2. Observations of 3mOs | 9 |
| 3.2.1. Intensity vs Velocity | 9 |
| 3.2.2. Location in chromosphere: (x/y) | 9 |
| 3.2.3. Location in chromosphere: height (z) | 9 |
| 3.3. Physical mechanism that generates the 3mOs | 9 |
| 3.3.1. Slow, propagating magnetoacoustic waves from the photosphere | 11 |
| 3.3.2. Natural response of chromosphere at the acoustic cutoff frequency | 12 |
| 4. The flaring chromosphere | 13 |
| 4.1. Flare emission and evolution | 13 |
| 5. The Solar Dynamics Observatory (SDO) | 18 |
| 5.1. The Atmospheric Imaging Assembly (AIA) | 18 |
| 5.2. The Helioseismic and Magnetic Imager (HMI) | 18 |
| Introduction | 19 |
| Observations and data reduction | 22 |
| Analysis | 29 |
| Results and discussion | 31 |
| 7. Appendix: Physics background | 21 |
| 7.1. Waves | 21 |
| 7.2. The acoustic cutoff frequency | 21 |
| 7.2.1. Derivation of the cutoff frequency | 22 |

| | |
|------------------------------|----|
| 7.3. Coronal seismology | 24 |
| 7.3.1. Ideal MHD | 24 |
| 7.3.2. Characteristic speeds | 25 |
| 7.3.3. Kink waves | 26 |

ENHANCED CHROMOSPHERIC 3-MINUTE OSCILLATORY POWER ASSOCIATED WITH THE 2011-FEBRUARY-15 X2.2 FLARE

INTRODUCTION

Most of the radiative energy associated with solar flares is emitted from the chromosphere in the form of optical and UV emission, but the mechanism of energy transport from the magnetic reconnection site to the chromosphere and subsequent conversion to other forms remains unclear. The chromosphere has been observed to oscillate in response to an injection of energy, suggesting that the nature of such oscillations may reveal something about the nature of energy deposition and conversion associated with flares. In this paper, we aim to characterize the oscillatory response of the chromosphere before, during, and after an X-class flare with the goal of further investigating the “flaring chromosphere” and helping to constrain the origin of the persistent 3-minute oscillations in the chromosphere.

The 3-minute oscillations observed in the chromosphere have been attributed to the upward propagation of slow magnetoacoustic waves that originate in deeper layers of the solar atmosphere. The acoustic cutoff frequency at the base of the chromosphere, $\nu_0 \approx 5.6$ mHz (~ 3 minute period), effectively creates a barrier across which waves can travel only if their propagation frequency is higher than ν_0 . Another explanation is that the acoustic cutoff frequency is the natural frequency at which the chromospheric plasma will respond to a disturbance. This was predicted and shown numerically by a series of papers by [Sutmann & Ulmschneider \(1995a,b\)](#); [Sutmann et al. \(1998\)](#), and other studies by [Chae & Goode \(2015\)](#). Enhancement of oscillations close to a period of 3 minutes has since been observed associated with a variety of phenomena. [Kwak et al. \(2016\)](#) observed the response of the chromosphere to a downflow event using high-resolution spectra from the *Interface Region Imaging Spectrograph* (*IRIS*; [De Pontieu et al. \(2014\)](#)). ? detected a different type of oscillations above an active region associated with a flare.

[Milligan et al. \(2017\)](#) observed an enhancement in the 3-minute power from thermal emission that was not present in X-ray emission associated with the flare. supporting the prediction that the chromosphere naturally responds to an impulsive disturbance at the acoustic cutoff frequency.

[Kumar & Ravindra \(2006\)](#) observed an enhancement in velocity oscillations between 5 and 6.5 mHz in emission in close proximity to the source of HXR emission in RHESSI images, and interpreted this locally concentrated enhancement as energy injection by non-thermal particles.

[Brosius & Daw \(2015\)](#) studied UV stare spectra of an M-class flare in Si IV, C I, and O IV lines, and reported four complete intensity fluctuations with periods around 171 seconds, in further support of the model of energy injection in the chromosphere by non-thermal particle beams.

The 3-minute period falls within the typical range of periods observed in the form of small-scale fluctuations known as quasi-periodic pulsations (QPPs). QPPs have been observed in flare emission throughout all stages and across all wavelength bands, and are considered to be intrinsic signatures of flare dynamics. In particular, QPPs in thermal emission from the chromosphere may provide a tool for investigating the transportation of energy from the flare site down into the chromosphere ([Inglis et al. 2015](#)).

[Sych et al. \(2009\)](#) suggested that the leakage of umbral 3-minute oscillations into the upper atmosphere was the cause of flaring QPPs, supported by observations of a similar periodicity in the flare emission.

[Monsue et al. \(2016\)](#) observed an enhancement of frequencies between 1 and 8 mHz associated with an M- and X-class flare in H α emission integrated over the AR, but investigation of subregions revealed an enhancement at low frequencies (1-2 mHz) in inner flare regions before and after the flare, and a suppression of oscillatory power over all frequencies between 1 and 8 mHz during the main phases.

[Awasthi et al. \(2018\)](#) found two distinct pre-flare phases, beginning with non-thermal particles and evolving into a thermal conduction front. [Fletcher et al. \(2013\)](#) studied both the thermal and non-thermal response of the chromosphere during the early stages of an M-class flare, and found the main flux to originate from a different location from the initial brightenings.

The goal of the present study is to investigate the location of power enhancement before, during, and after a flare. The extra time will allow comparison between flaring and non-flaring chromosphere to distinguish whether the plasma is oscillating at the natural frequency of the chromosphere or responding to an impulsive injection of energy. The location of power enhancement will help probe the nature of the energy deposition at various phases.

Here we present the spatial and temporal evolution of 3-minute power in the chromosphere during the *GOES* X-class flare that occurred on 15 February 2011. The Atmospheric Imaging Assembly (AIA; [Lemen et al. \(2012\)](#)) on board the *Solar Dynamics Observatory* (SDO; [Pesnell et al. \(2012\)](#)) provides images with a spatial size scale of 0.6" per pixel and 24-second cadence in thermal UV emission from two channels that sample the lower atmosphere. These data allow the computation of spatially resolved power maps centered on the frequency of interest. The flare, data, and methodology

are described in §???. Results are presented and discussed in §???. We conclude in §?? with key preliminary findings and plans for the continuation and development of this work.

OBSERVATIONS AND DATA REDUCTION

The 2011 February 15 X2.2 flare occurred in NOAA active region (AR) 11158 close to disk center during solar cycle 24 (SOL2011-02-15T01:56). The AR was composed of a quadrupole: two sunspot pairs (four sunspots total). The X-flare occurred in a delta-spot composed of the leading spot of the southern pair and the trailing spot of the northern pair. It started at 01:44UT, peaked at 01:56UT, and ended at 02:06UT, as determined by the soft X-ray flux from the *Geostationary Operational Environmental Satellite* (*GOES*-15; [Viereck et al. \(2007\)](#)). The impulsive phase lasted about 10 minutes. Data covering 5 hours centered on this flare were used for the analysis. This data includes a C-class flare that occurred between 00:30 and 00:45 UT on 15 February 2011.

SDO/AIA obtains full disk images throughout the solar atmosphere, using narrow band filters centered on 10 different wavelengths, two of which provide measurements of thermal UV emission from the [chromosphere](#). The 1700Å channel [mostly contains](#) continuum emission from the temperature minimum, and the 1600Å channel [covers](#) both continuum emission and the C IV spectral line in the upper photosphere and transition region. Both channels have a cadence of 24 seconds and [spatial size scale](#) of 0.6 arcseconds per pixel.

Data from the Helioseismic and Magnetic Imager (HMI; [Scherrer et al. \(2012\)](#)), also on board *SDO*, is used to [study](#) potential correlations between magnetic field strength and oscillatory behavior in the chromosphere. HMI obtains full disk data in the form of line-of-sight magnetograms, vector magnetograms, Doppler velocity, and continuum intensity, measured at the Fe I absorption line at 6173Å with a passband width of 0.076Å. Each [data product](#) has a cadence of 45 seconds (with the exception of the vector magnetograms, at 135 seconds), and [spatial size scale](#) of 0.5 arcseconds per pixel ([Schou et al. 2012](#)).

The standard data reduction routine *aia_prep.pro* from solarsoft was [applied to all data](#).

Figure 4 shows light curves for the full 5-hour time series from 00:00 to 04:59 on 2011-February-15. The top panel shows both AIA channels. The bottom panel shows both SXR channels from *GOES*-15 at 1-8Å (black curve) and 0.5-4Å (pink curve). A small C-flare occurred before the X-flare between 00:30 and 00:45 UT, and two small events occurred after the X-flare, between 03:00 and 03:15, and between 04:25 and 04:45.

Pre-flare images of the full disk are shown in Figure 2, along with a 300x198 arcsecond subset of the data centered on AR 11158. [This subset was extracted and aligned by cross correlation](#) ([McAteer et al. 2003, 2004](#)). Images were scaled to improve contrast using the *aia_intscale.pro* routine from *sswidl*. The magnetic configuration

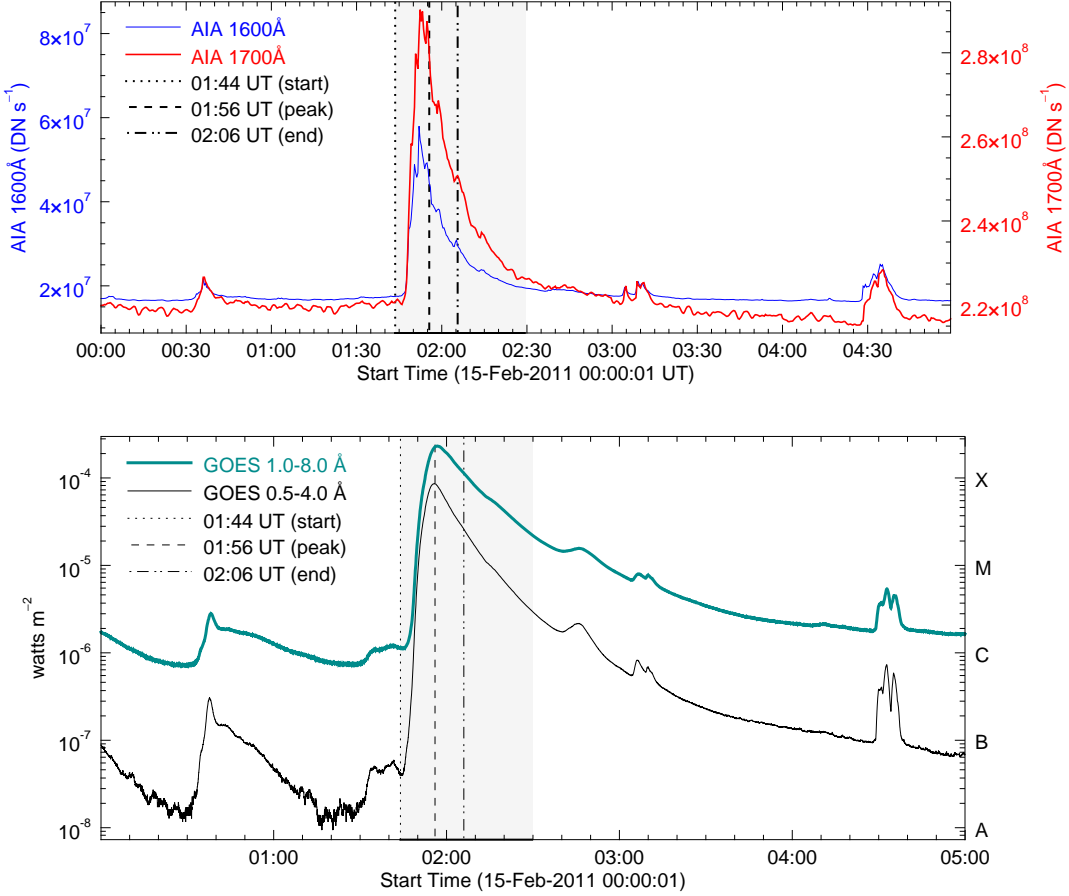


Figure 1. Top: Light curves of the UV continuum emission from AIA 1600Å (blue curve) and AIA 1700Å (red curve), integrated over the flare region in AR 11158. Bottom: Light curves observed by the *GOES-15* satellite channels 1-8Å (black curve) and 0.5-4Å (pink curve), scaled as $\log(\text{flux})$ to enable visibility of the increases during smaller events before and after the main X-flare.

of the quadrupole is clear in the HMI magnetograms. The northern pair will be designated as AR_1 and the southern pair will be designated as AR_2. Sunspots in the northern pair will be designated as AR_1p (positive polarity) and AR_1n (negative polarity). Sunspots in the southern pair will be designated as AR_2p (positive polarity) and AR_2n (negative polarity).

Both AIA channels saturated (≥ 15000 counts) in the center during the peak of the X-class flare, and a few pixels also saturated during the smaller events before and after. Affected pixels were all contained within the 300x198 arcsecond subset of data throughout the duration of the time series. Four images from the 1700Å channel on AIA were missing, between the images with start times at 00:59:53.12, 01:59:29.12, 02:59:05.12, and 03:58:41.12, and the following images, each with start times 48 seconds after the previous image. Since the gaps in data were separated

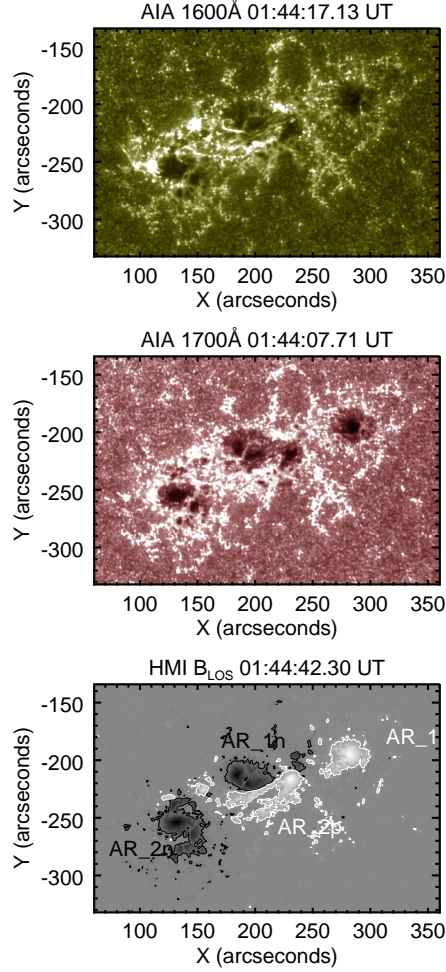


Figure 2. Active region 11158 in AIA 1600Å (top), AIA 1700Å (middle), and HMI LOS magnetogram (bottom) on 2011-February-15. The white and black contours outline positive (+300 Gauss) and negative (-300 Gauss) polarities, respectively. The two sunspots in the northern pair are labeled AR_1p (leading sunspot) and AR_1n (trailing sunspot). The two sunspots in the southern pair are labeled AR_2p (leading sunspot) and AR_2n (trailing sunspot).

by an hour, it was reasonable to approximate missing images by averaging the two adjacent images.

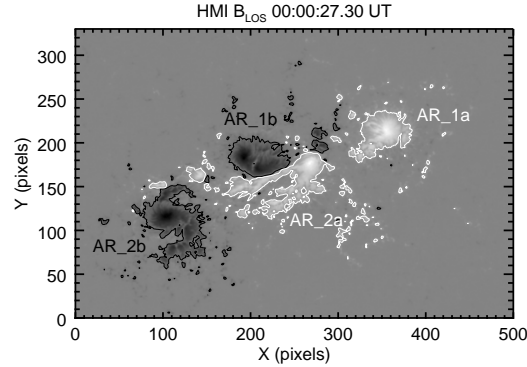


Figure 3. HMI LOS magnetogram. White and black contours outline positive (+300 Gauss) and negative (-300 Gauss) polarities, respectively. The two sunspots in the northern pair are labeled AR_1a (leading sunspot) and AR_1b (trailing sunspot). The two sunspots in the southern pair are labeled AR_2a (leading sunspot) and AR_2b (trailing sunspot).

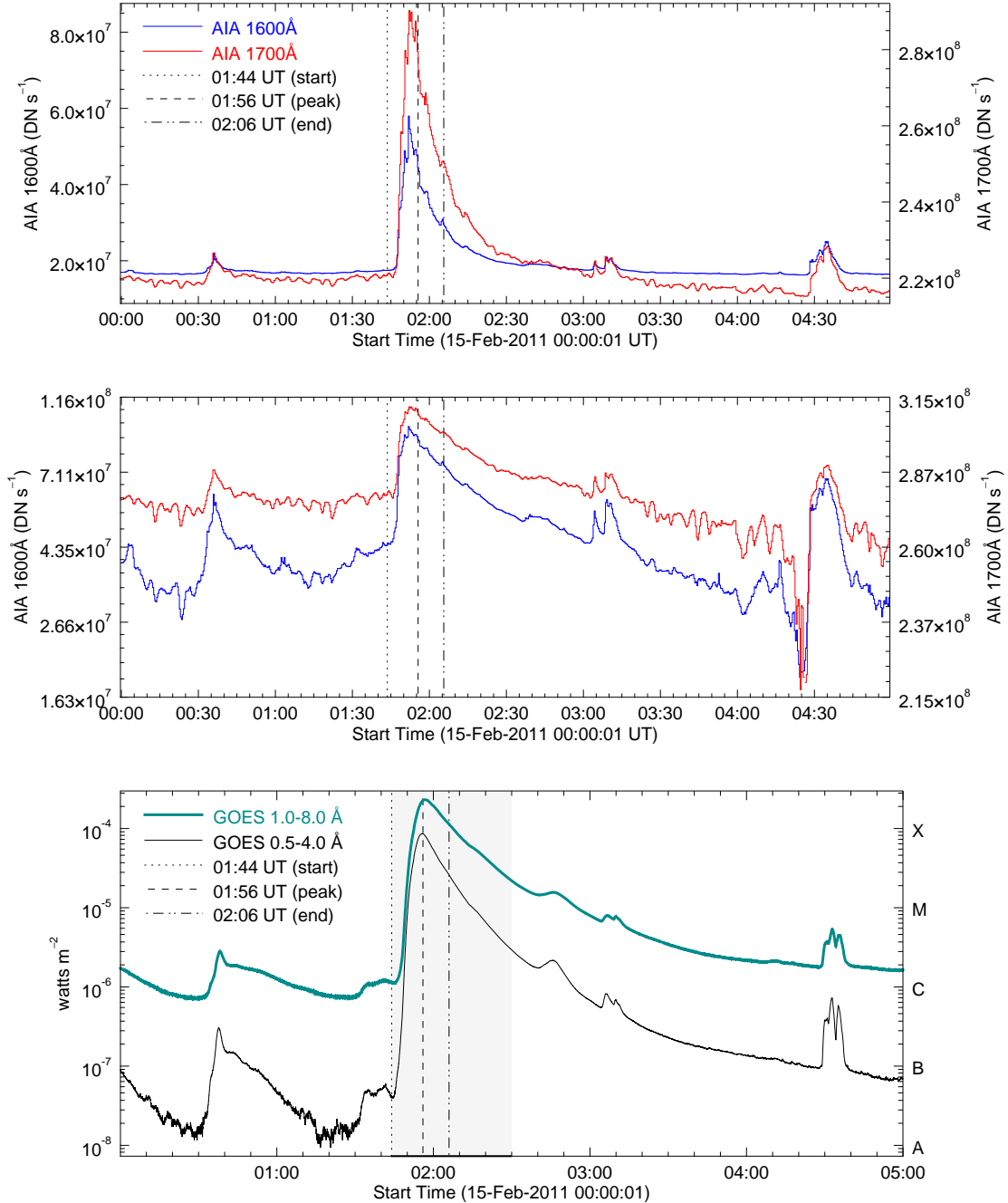


Figure 4. Top: Light curves of the UV continuum emission from AIA 1600Å (blue curve) and AIA 1700Å (red curve), integrated over the flare region in AR 11158. Middle: Same as top, but scaled as log(flux). Bottom: Light curves from *GOES-15* channels 1-8Å (black curve) and 0.5-4Å (pink curve), scaled as log(flux) to enable visibility of the increases during smaller events before and after the main X-flare.

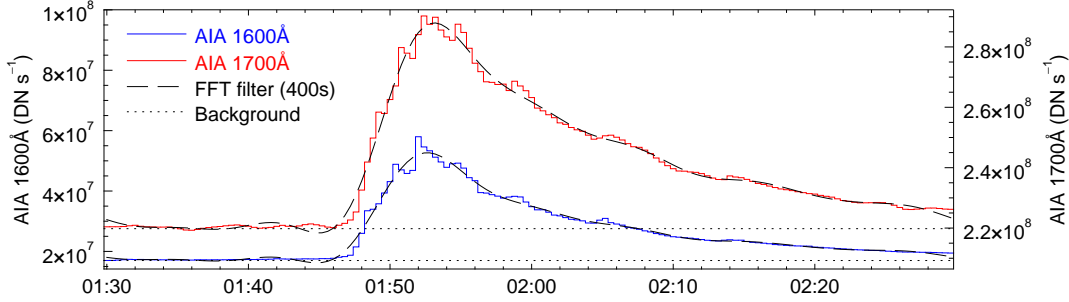


Figure 5. Light curves of AIA 1600Å and AIA 1700Å, overlaid with same light curves after applying a FFT filter with a period cutoff of 400 seconds.

Plot of detrended data goes here. Threshold = lower limit on frequency to get rid of global variations (e.g. the flare) and keep high-frequency variations, like QPPs. Sun Dec 2 12:37:06 MST 2018

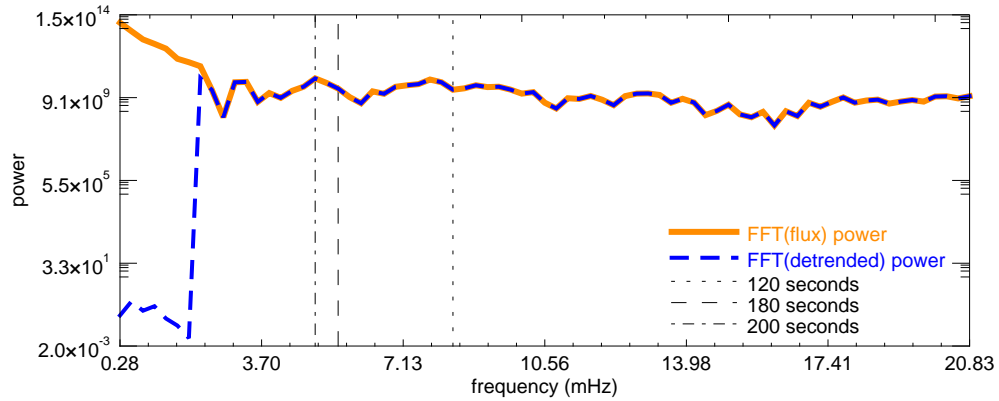


Figure 6. Power spectrum from AIA 1600Å flux between 1:30 and 2:30 UT. The orange curve is the power from the raw data, and the blue curve is the power from flux after applying an FFT high-pass filter to remove variations with periods longer than 400 seconds, such as the global flare curve, which dominates the spectrum at low frequencies.

Table 6.1 shows the time ranges covered by each time period of interest, and the processes that occurred during that time.

Table 6.1. Pre-flare, X-flare, and post-flare things that happened

| Phase | Indices | Time range (UT) | What's happening |
|--------|---------|-----------------|---|
| Before | 0:63 | 00:00–00:25 | blip at very beginning |
| ... | 16:79 | 00:07–00:32 | Quiet |
| ... | 27:90 | 00:11–00:36 | pre-flare through C-flare peak |
| ... | 80:143 | 00:32–00:57 | Centered on C-flare |
| ... | 90:153 | 00:36–01:01 | C-flare peak (close to previous t-seg; start to peak ~4 min!) |
| ... | 147:200 | 00:59–01:24 | Through where em. back to pre-Cflare levels |
| ... | ... | ... | also centered on brief flux increase at ~1:01–1:05 (2b) |
| ... | 175:238 | 01:10–01:35 | Quiet, cleared of obvious emission increase |
| ... | 197:260 | 01:19–01:44 | BP in (1a), been there since 00:30, |
| ... | ... | ... | though no noticeable increase in flux from this SS |
| During | ... | 01:45–02:30 | ... |
| After | ... | 02:30–04:59 | ... |

ANALYSIS

The technique used to calculate power maps as functions of space and time is similar to that employed by [Jackiewicz & Balasubramaniam \(2013\)](#) and further employed by [Monsue et al. \(2016\)](#). The general method is as follows: For a data set of N images, each power map $P(x, y, t_i)$ is generated by applying a Fourier transform to every pixel at (x, y) in the temporal direction, from t_i to $t_i + T$, where T is the length of the time segment. The power is averaged over a frequency band $\Delta\nu$ of user-defined width, centered on the frequency of interest. This process is repeated at every timestep, for starting times from t_0 to t_{N-N_T} .

The data set for AR 11158 consisted of $N = 749$ images (5 hours) of AIA observations in each channel. Each time segment T was set to 64 images (~ 25.6 minutes). The value of T was chosen based on a balance between sufficient length to obtain frequencies close to that of the 3-minute period and not so long as to lose information on timescales over which the 3-minute power was previously observed to change. Each Fourier transform was applied without detrending the data since the frequency of interest was well outside the global flare signal. (As a check on this, a Fourier filter was applied with a cutoff period above 400 seconds. The power spectra for the periods of interest did not change.) If a saturated pixel was encountered in any segment t_i to $t_i + T$, it was excluded from the power map for that time segment, and the location (x, y) of that pixel was set to zero.

The frequency bandwidth $\Delta\nu$ was set to 1 mHz centered on $\nu \sim 5.6$ mHz. This is consistent with similar techniques applied in previous studies. For instance, [Stangalini et al. \(2011\)](#) used a 1-mHz frequency bandpass between 4.8 mHz (208.3 seconds) and 5.8 mHz (172.4 seconds) when calculating power maps around 5.6 mHz for the chromosphere and photosphere. [Tripathy et al. \(2018\)](#) also used a band of 1 mHz over 0.1-mHz steps from 1 to 10.5 mHz. [Reznikova et al. \(2012\)](#) used a bandpass of only 0.4 mHz...

With these input parameters, a frequency resolution $\partial\nu$ of ~ 0.65 mHz was obtained. Two frequencies were obtained within $\Delta\nu$ at 5.21 mHz (192.00 seconds) and 5.86 mHz (170.67 seconds).

The average power over $\Delta\nu$ for each unsaturated pixel in time segment T from t_i to $t_i + T$ was taken to be the 3-minute power in each power map. Since only two frequencies were obtained within $\Delta\nu$, and were centered around the frequency of interest, the average was computed without the application of a filter.

Power maps representing the 3-minute power over NOAA AR 11158 in space and time were obtained at every starting point in the time series (up to $N - T$) by applying a

Fourier transform to the signal from each pixel, and averaging the power within the 1-mHz frequency bandwidth $\Delta\nu$ centered around 5.6 mHz (3 minutes).

RESULTS AND DISCUSSION

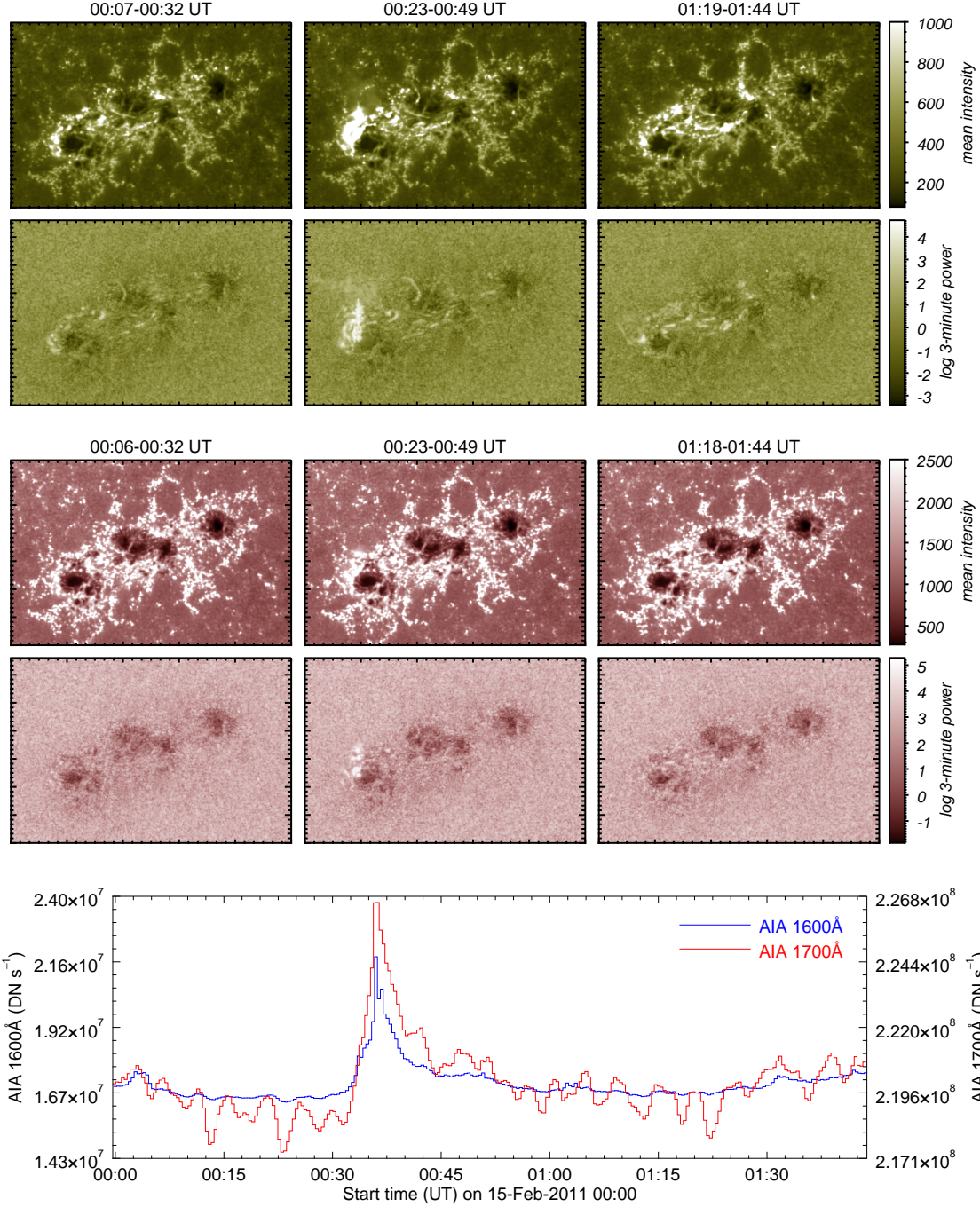


Figure 7. Spatial distribution of 3-minute power (arbitrary instrumental units) for AIA 1600Å (top) and AIA 1700Å (bottom) with the central frequency at 5.6 mHz (± 0.5 mHz). The x and y dimensions are the same as the images in Figure 2.

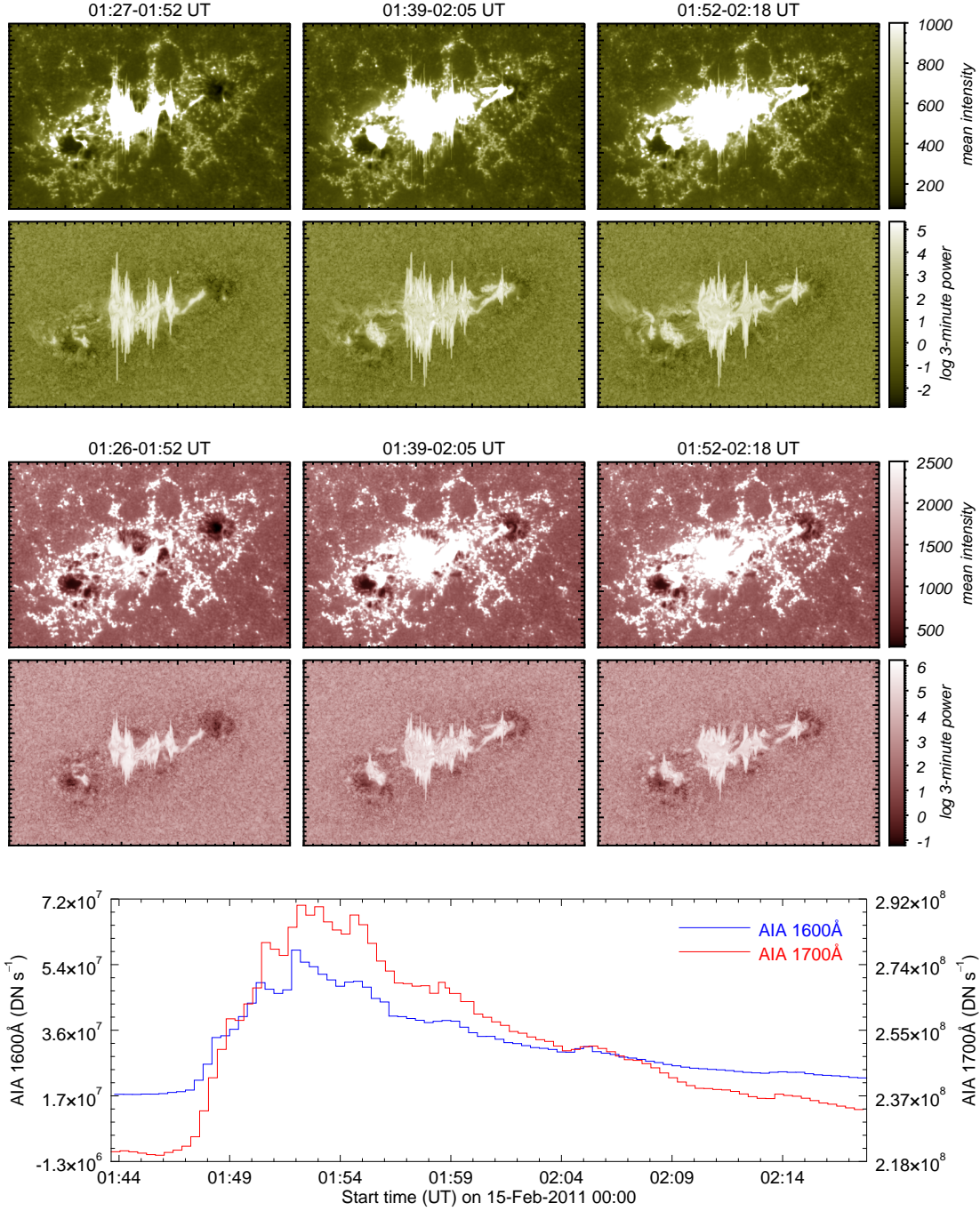


Figure 8. Mid-flare power maps.

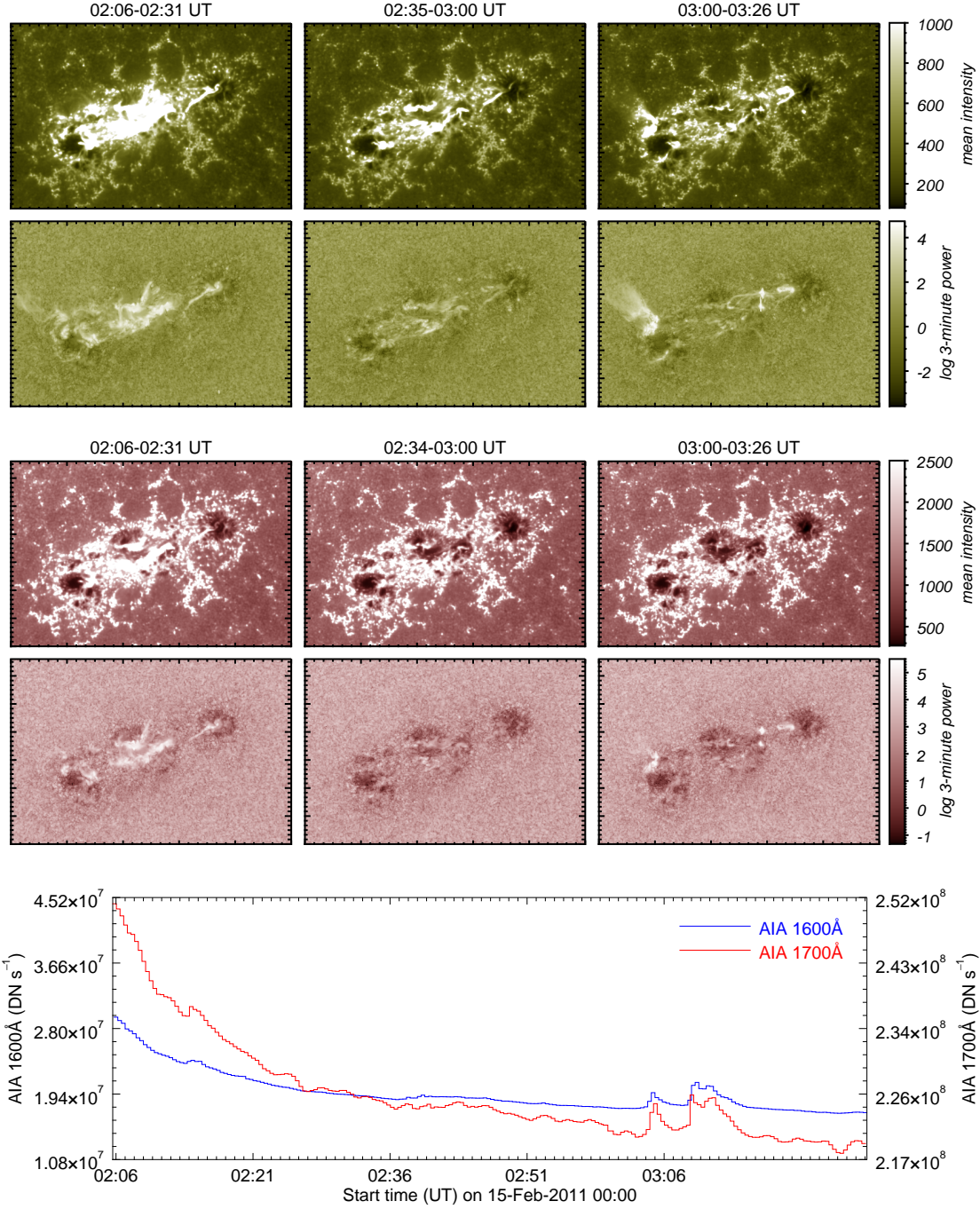


Figure 9. Post-flare power maps.

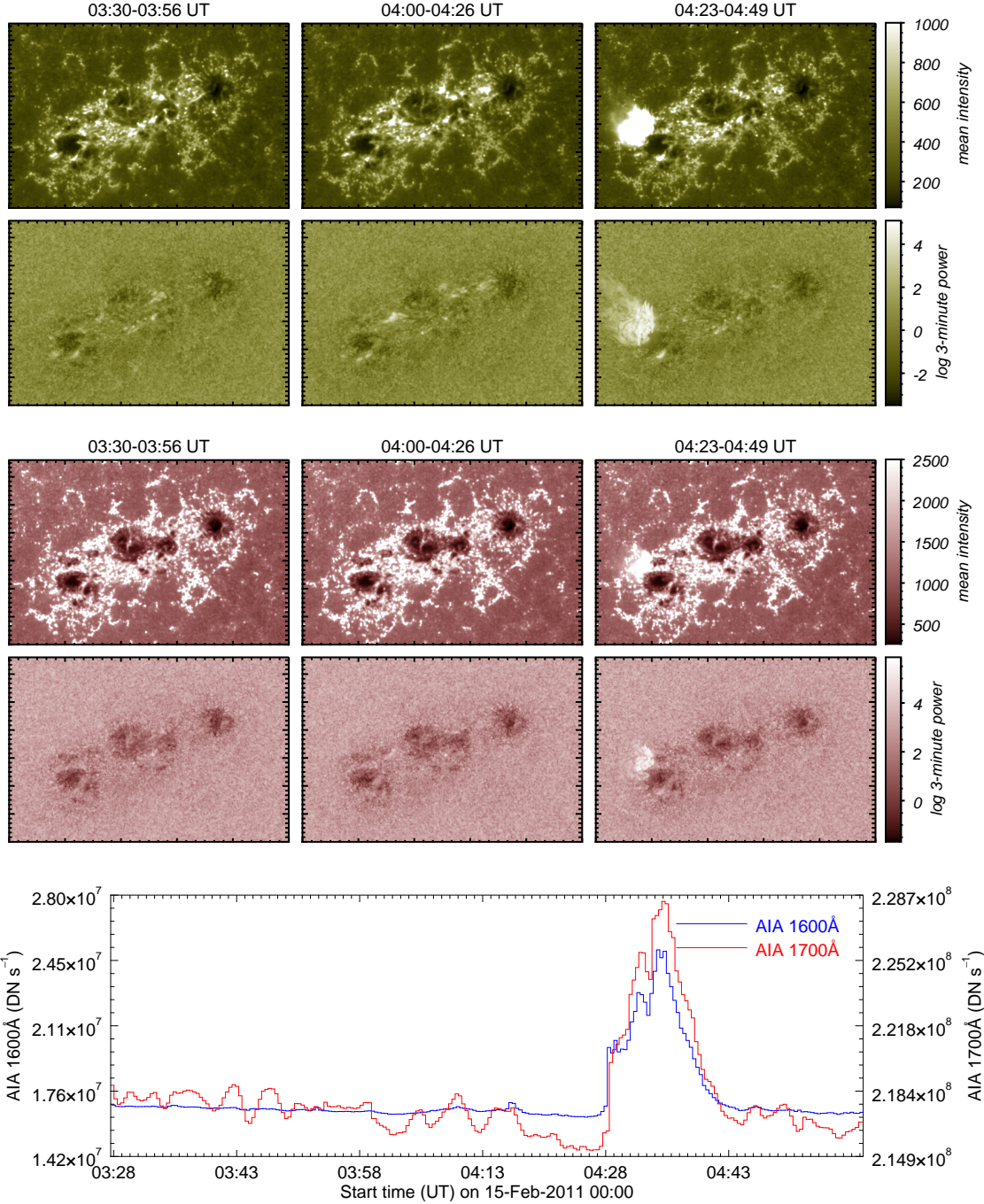


Figure 10. Post-flare power maps.

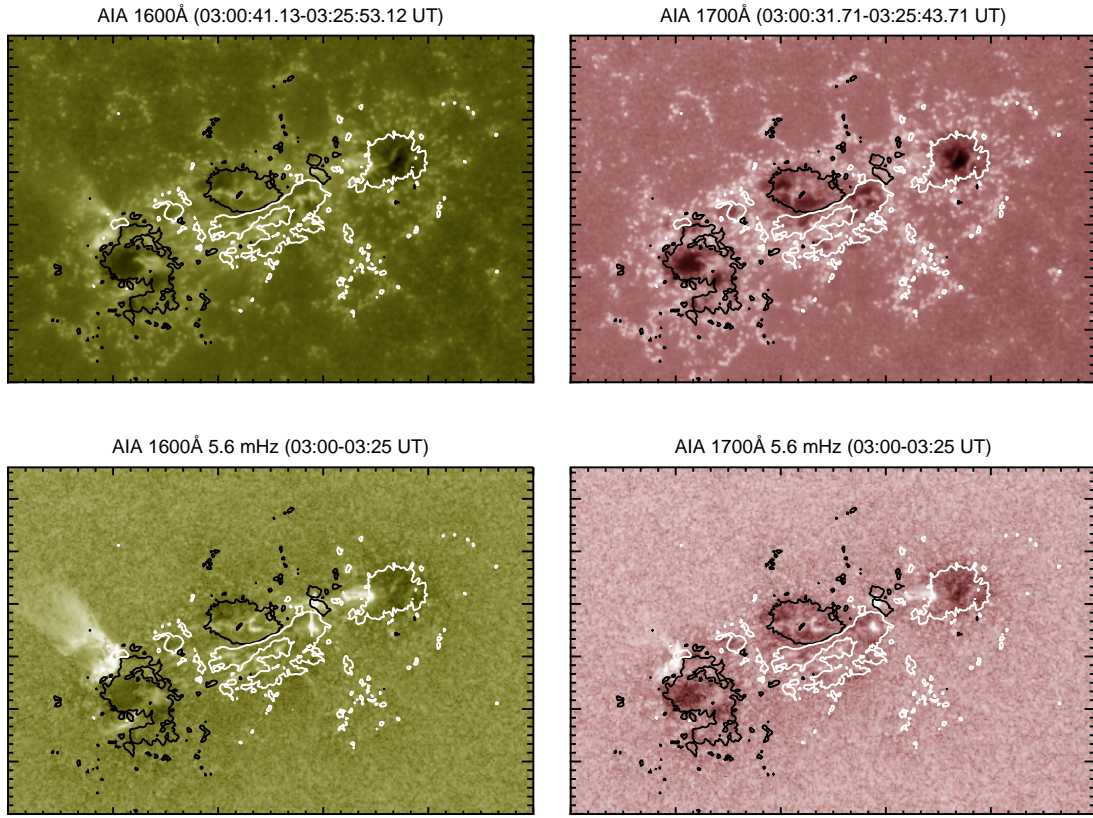


Figure 11. Post-flare power maps overlaid with contours showing the approximate location of the B_{LOS} at ± 300 Gauss. White and black contours represent positive and negative polarity, respectively.

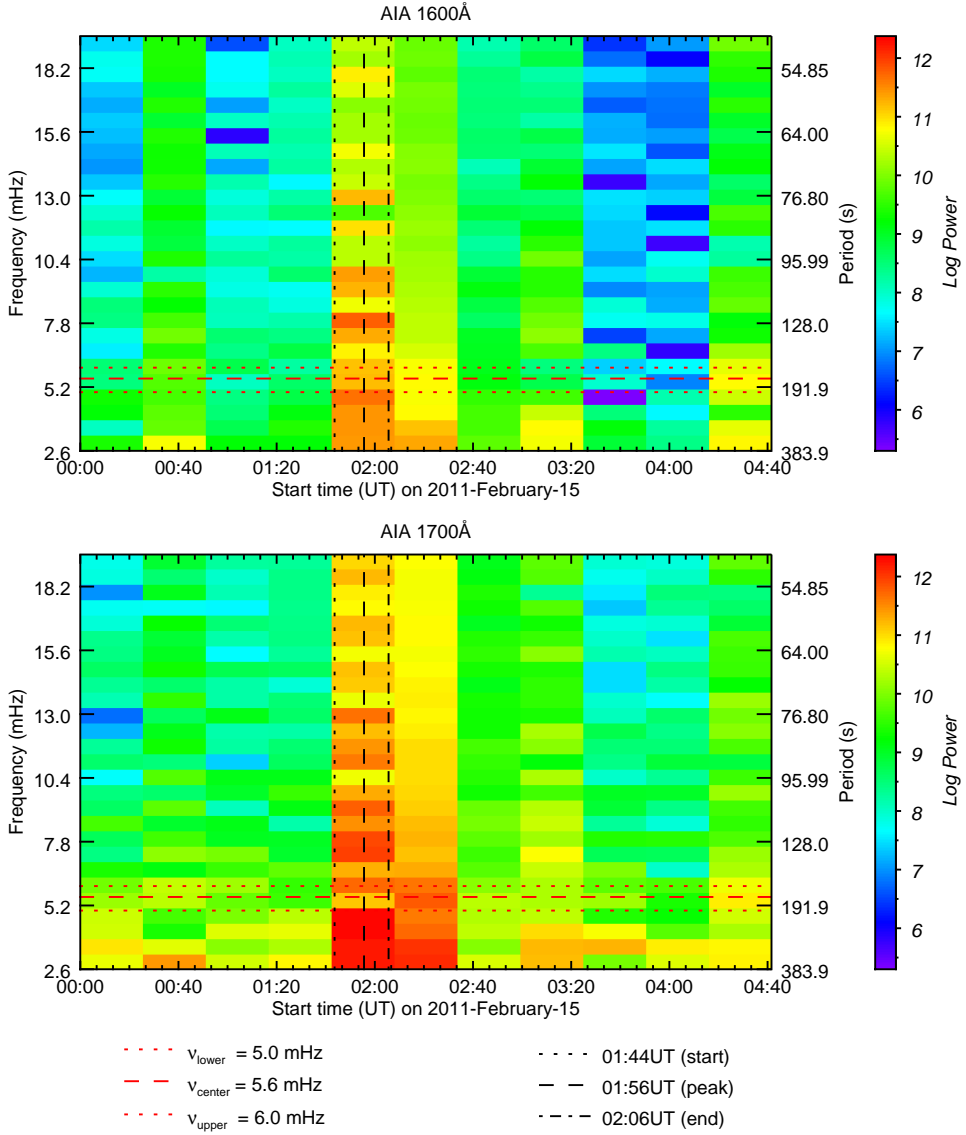


Figure 12. Time-frequency power plots from AIA 1600 \AA (top panel) and AIA 1700 \AA (bottom panel), obtained by applying a Fourier transform to integrated emission from NOAA AR 11158 in discrete time increments of 64 frames (~ 25.6 minutes) each. The dashed horizontal line marks the central frequency ν_c at ~ 5.6 mHz, corresponding to a period of 3 minutes. The dotted horizontal lines on either side of ν_c mark the edges of the frequency bandpass $\Delta\nu = 1$ mHz. The vertical lines mark the flare, start, peak, and end times as determined by *GOES*. The power is scaled logarithmically and over the same range in both channels. Note that the x-axis labels do not necessarily line up with the boundaries of the data columns.

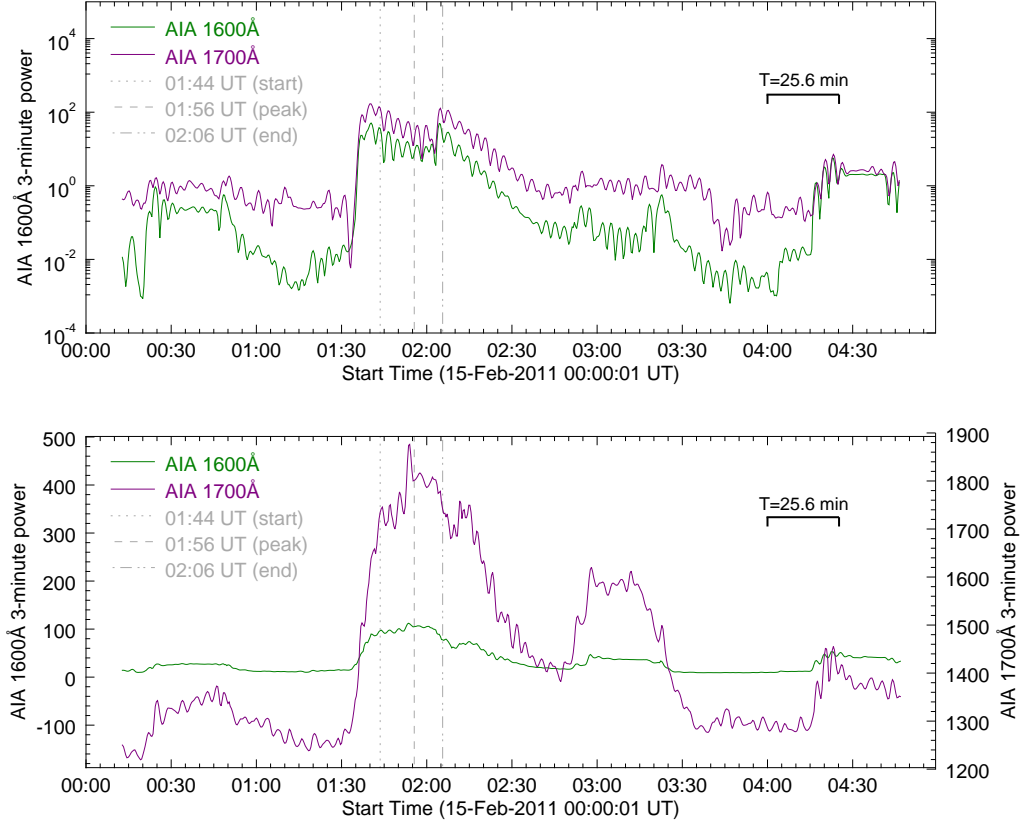
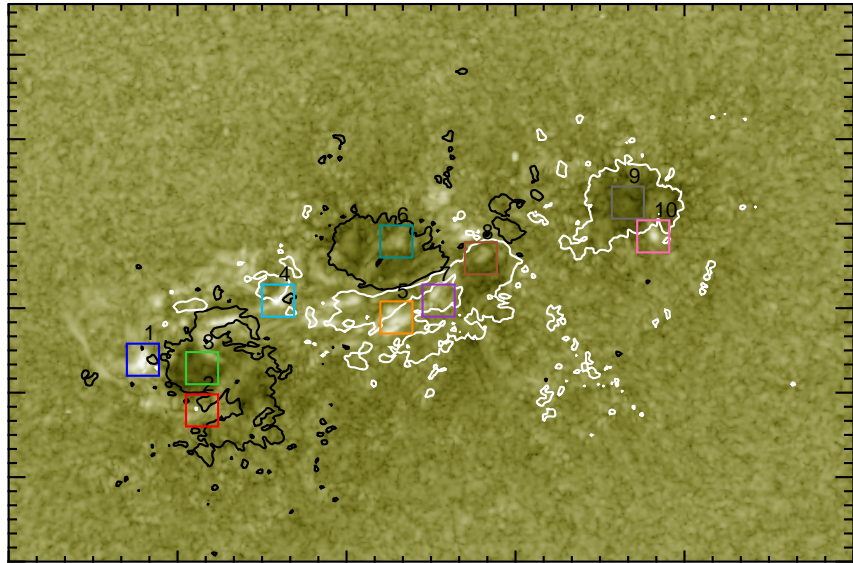
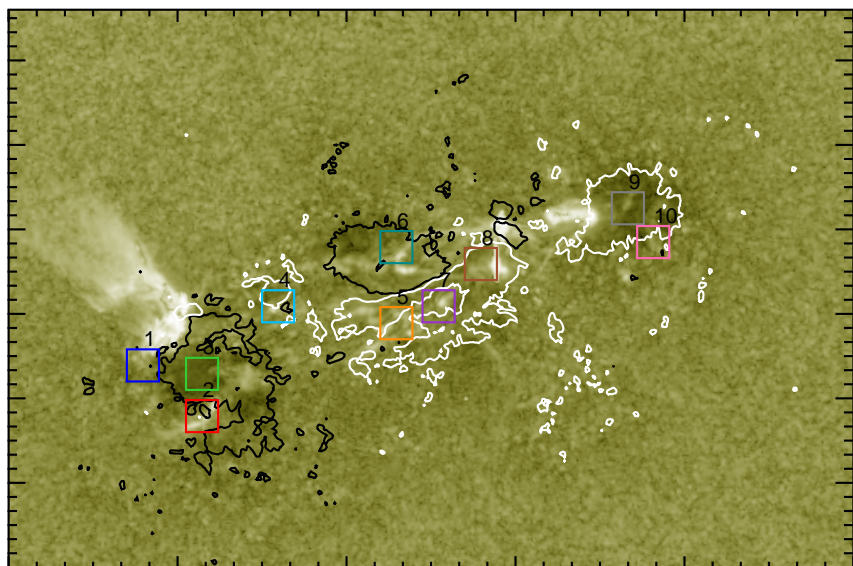


Figure 13. Temporal evolution of the 3-minute power $P_{3\text{min}}(t)$ in AIA 1600Å (blue curve) and AIA 1700Å (red curve). Top: $P(t)$ obtained by applying a Fourier transform to the integrated flux from AR 11158. Bottom: $P(t)$ per unsaturated pixel, obtained by summing over power maps. Each point in time is plotted as a function of the center of the time segment over which the Fourier transform was applied to obtain the power map over which the point was summed. The vertical dashed lines mark the *GOES* start, peak, and end times of the flare at 01:44, 01:56, and 02:06 UT, respectively.

AIA 1600Å 5.6 mHz (01:19-01:44 UT)



AIA 1600Å 5.6 mHz (03:00-03:25 UT)



CONCLUSIONS

In this work, we have presented spatial distribution of the 3-minute oscillations associated with the X-class flare that occurred in AR11158 on 15 February 2011. Key points are as follows:

1. Small, distinct regions of enhanced power show that the chromospheric plasma does not oscillate as one body.
2. Location relative to AR same as enhanced intensity associated with the flare, which supports the theory of oscillation in response to energy injection via accelerated non-thermal particles.
3. Variation in enhancement location throughout flare phases indicates a possible change in source of energy input.

Future work will involve smaller flares to avoid saturation issues. It is possible that important spatial information is contained in location of the flare core, but cannot be extracted due to the saturation in the pixels. Saturation does not occur as often for flares of less powerful classes. Since several of the data images saturated during the main phase of the flare, spatial information cannot be obtained at the core location of the flare. It may be worthwhile to apply these methods to a less powerful flare.

The temporal behavior of oscillations during the main flare remains inconclusive due to the necessary balance between temporal and frequency resolution. Techniques to improve temporal resolution, such as the standard wavelet analysis presented by [Torrence & Compo \(1998\)](#), will allow study of chromospheric behavior on timescales comparable to those over which flare dynamics are known to occur.

The pre-flare data shown in this work may not be the best representation since another, smaller flare took place in the middle of it. It may be worthwhile to obtain more data at earlier times

Acknowledgements: ?

REFERENCES

- Awasthi, A. K., Rudawy, P., Falewicz, R., Berlicki, A., & Liu, R. 2018.
<https://arxiv.org/abs/1804.02632>
- Battaglia, M., Kleint, L., Krucker, S., & Graham, D. 2015, *Astrophys. J.*, 813, 113, doi: [10.1088/0004-637X/813/2/113](https://doi.org/10.1088/0004-637X/813/2/113)
- Beckers, J. M., & Schultz, R. B. 1972, *Sol. Phys.*, 27, 61, doi: [10.1007/BF00151770](https://doi.org/10.1007/BF00151770)
- Beckers, J. M., & Tallant, P. E. 1969, *Sol. Phys.*, 7, 351, doi: [10.1007/BF00146140](https://doi.org/10.1007/BF00146140)
- Boerner, P., Edwards, C., Lemen, J., et al. 2012, *Sol. Dyn. Obs.*, 9781461436, 41, doi: [10.1007/978-1-4614-3673-7_4](https://doi.org/10.1007/978-1-4614-3673-7_4)
- Bogdan, T. J., & Judge, P. G. 2006, *Philos. Trans. R. Soc.*, 364, 313, doi: [10.1098/rsta.2005.1701](https://doi.org/10.1098/rsta.2005.1701)
- Brosius, J. W., & Daw, A. N. 2015, *Astrophys. J.*, 810, doi: [10.1088/0004-637X/810/1/45](https://doi.org/10.1088/0004-637X/810/1/45)
- Brosius, J. W., Daw, A. N., & Inglis, A. R. 2016, *Astrophys. J.*, 830, 101, doi: [10.3847/0004-637X/830/2/101](https://doi.org/10.3847/0004-637X/830/2/101)
- Brynildsen, N., Leifsen, T., Kjeldseth-Moe, O., Maltby, P., & Wilhelm, K. 1999, *JApjl*, 511, L121, doi: [10.1086/311854](https://doi.org/10.1086/311854)
- Brynildsen, N., Maltby, P., Fredrik, T., & Kjeldseth-Moe, O. 2004. <http://adsabs.harvard.edu/abs/2004ESASP.547...45B>
- Chae, J., & Goode, P. R. 2015, *Astrophys. J.*, 808, 118, doi: [10.1088/0004-637X/808/2/118](https://doi.org/10.1088/0004-637X/808/2/118)
- De Moortel, I., Ireland, J., & Walsh, R. 2000, *Astron. Astrophys.*, 355, L23, doi: [10.1063/1.1324943](https://doi.org/10.1063/1.1324943)
- De Pontieu, B., Title, A. M., Lemen, J. R., et al. 2014, *Sol. Phys.*, 289, 2733, doi: [10.1007/s11207-014-0485-y](https://doi.org/10.1007/s11207-014-0485-y)
- Felipe, T., Khomenko, E., & Collados, M. 2010, *Astrophys. J.*, 719, 357, doi: [10.1088/0004-637X/719/1/357](https://doi.org/10.1088/0004-637X/719/1/357)
- Fleck, & Schmitz. 1991, *Astron. Astrophys.*, 250, 235
- Fletcher, L., Hannah, I. G., Hudson, H. S., & Innes, D. E. 2013, *Astrophys. J.*, 771, 104, doi: [10.1088/0004-637X/771/2/104](https://doi.org/10.1088/0004-637X/771/2/104)
- Giovanelli. 1972, *Sol. Phys.*, 27, 71
- Hoyng, P., Duijveman, A., Machado, M. E., et al. 1981, *Astrophys. J. Lett.*, 246, L155, doi: [10.1086/183574](https://doi.org/10.1086/183574)
- Hudson, H. 2007, *Phys. Chromospheric Plasmas*, 368, 365.
<https://arxiv.org/abs/0704.0823>
- Inglis, A. R., Ireland, J., & Dominique, M. 2015, *Astrophys. J.*, 798, 108, doi: [10.1088/0004-637X/798/2/108](https://doi.org/10.1088/0004-637X/798/2/108)
- Jackiewicz, J., & Balasubramaniam, K. S. 2013, *Astrophys. J.*, 765, 15, doi: [10.1088/0004-637X/765/1/15](https://doi.org/10.1088/0004-637X/765/1/15)
- Jensen, & Orrall, F. Q. 1963
- Judge, P. 2006, *Sol. MHD Theory Obs. A High Spat. Resolut. Perspect.*, 354, 259.
<https://arxiv.org/abs/0701379>
- Kalkofen, W. P. G. S. M. 1994, *Astron. Astrophys.*, 284, 976
- Kumar, B., & Ravindra, B. 2006, *J. Astrophys. Astron.*, 27, 425, doi: [10.1007/BF02709368](https://doi.org/10.1007/BF02709368)
- Kwak, H., Chae, J., Song, D., et al. 2016, *Astrophys. J.*, 821, L30, doi: [10.3847/2041-8205/821/2/L30](https://doi.org/10.3847/2041-8205/821/2/L30)
- Lemen, J. R., Title, A. M., Akin, D. J., et al. 2012, *Sol. Phys.*, 275, 17
- Maltby, P., Brynildsen, N., Fredrik, T., Kjeldseth-Moe, O., & Wilhelm, K. 1999, *Sol. Phys.*, 190, 437
- McAteer, R. T. J., Gallagher, P. T., Bloomfield, D. S., et al. 2004, *Astrophys. J.*, 602, 436, doi: [10.1086/380835](https://doi.org/10.1086/380835)
- McAteer, R. T. J., Gallagher, P. T., Williams, D. R., et al. 2003, *Astrophys. J.*, 587, 806, doi: [10.1086/368304](https://doi.org/10.1086/368304)
- Milligan, R. O., Fleck, B., Ireland, J., Fletcher, L., & Dennis, B. R. 2017, *Astrophys. J.*, 848, L8, doi: [10.3847/2041-8213/aa8f3a](https://doi.org/10.3847/2041-8213/aa8f3a)
- Monsue, T., Hill, F., & Stassun, K. G. 2016, *Astron. J.*, 152, 81, doi: [10.3847/0004-6256/152/4/81](https://doi.org/10.3847/0004-6256/152/4/81)
- Nakariakov, V. M., & Verwiche, E. 2005, *Living Rev. Sol. Phys.*, 2, doi: [10.12942/lrsp-2005-3](https://doi.org/10.12942/lrsp-2005-3)
- Orrall, F. Q. 1966, 917
- OShea, E., Muglach, K., & Fleck, B. 2002, 664, 642, doi: [10.1051/0004-6361](https://doi.org/10.1051/0004-6361)

- Pesnell, W. D., Thompson, B., & Chamberlin, P. 2012, Sol. Dyn. Obs., 9781461436, 1, doi: [10.1007/978-1-4614-3673-7](https://doi.org/10.1007/978-1-4614-3673-7)
- Priest, E. R., & Longcope, D. W. 2017, Sol. Phys., 292, 1, doi: [10.1007/s11207-016-1049-0](https://doi.org/10.1007/s11207-016-1049-0)
- Reznikova, V. E., Shibasaki, K., Sych, R. A., et al. 2012, Astrophys. J., 746, 119, doi: [10.1088/0004-637X/746/2/119](https://doi.org/10.1088/0004-637X/746/2/119)
- Scherrer, P. H., Schou, J., Bush, R. I., et al. 2012, Sol. Dyn. Obs., 9781461436, 207, doi: [10.1007/978-1-4614-3673-7_10](https://doi.org/10.1007/978-1-4614-3673-7_10)
- Scheuer, M. A., & Thomas, J. H. 1981, Sol. Phys., 71, 21, doi: [10.1007/BF00153603](https://doi.org/10.1007/BF00153603)
- Schou, J., Scherrer, P. H., Bush, R. I., et al. 2012, Sol. Dyn. Obs., 9781461436, 229, doi: [10.1007/978-1-4614-3673-7_11](https://doi.org/10.1007/978-1-4614-3673-7_11)
- Stangalini, M., Del Moro, D., Berrilli, F., & Jefferies, S. M. 2011, 65, 1, doi: [10.1051/0004-6361/201117356](https://doi.org/10.1051/0004-6361/201117356)
- Sutmann, G., Musielak, Z. E., & Ulmschneider, P. 1998, Astron. Astrophys., 340, 556
- Sutmann, G., & Ulmschneider, P. 1995a, Astron. Astrophys., 294, 232
- . 1995b, Astron. Astrophys., 294, 241
- Sych, R., Nakariakov, V. M., Karlicky, M., Anfinogentov, S., & Anfinogentov, S. 2009, Astron. Astrophys., 505, 791, doi: [10.1051/0004-6361/200912132](https://doi.org/10.1051/0004-6361/200912132)
- Tian, H., DeLuca, E., Reeves, K. K., et al. 2014, Astrophys. J., 786, 137, doi: [10.1088/0004-637X/786/2/137](https://doi.org/10.1088/0004-637X/786/2/137)
- Torrence, & Compo. 1998, Bull. Am. Meteorol. Soc., 79, 61
- Tripathy, S. C., Jain, K., Kholikov, S., et al. 2018, Adv. Sp. Res., 61, 691, doi: [10.1016/j.asr.2017.10.033](https://doi.org/10.1016/j.asr.2017.10.033)
- Viereck, R., Hanser, F., Wise, J., et al. 2007, 66890K, doi: [10.1117/12.734886](https://doi.org/10.1117/12.734886)
- Wittmann, A. 1969, Sol. Phys., 7, 366, doi: [10.1007/BF00146141](https://doi.org/10.1007/BF00146141)
- Woods, M. M., Harra, L. K., Matthews, S. A., et al. 2017, Sol. Phys., 292, doi: [10.1007/s11207-017-1064-9](https://doi.org/10.1007/s11207-017-1064-9)